

Intelligent Mode-Locked Single-Cavity Dual-Comb Laser Utilizing Time-Stretch Dispersive Fourier Transform Spectroscopy with Supplemental File

Pan Guo, Yuan Gao, Yongjie Pu, Zhigang Zhao, Zhenhua Cong and Sha Wang*

Abstract—As dual combs play a significant role in numerous high-precision measurements, their efficient generation has been widely researched. Although the single-cavity dual-comb generation can avoid the complex active stabilization methods, achieving and maintaining stable dual-comb mode locking within a single cavity remains a critical challenge. To break through this constraint, a two-part evaluation criterion containing a fitness function and a CNN-Transformer network is employed to achieve mode locking and classify the dual-comb mode-locked state. Simulated time-stretch dispersive Fourier transform (DFT) spectra are used as datasets, which simplifies the optimization process and does not rely on specific experimental data. A developed evolutionary algorithm (EA) for paddle-based motorized polarization controllers (MPCs) is proposed, enabling the intelligent attainment of dual-comb mode-locked states. A real-time library stores fitness and MPC angles, facilitating mode-locked state achievement within 2 seconds. Finally, long term running of dual-comb mode locking is ensured by a random collision algorithm utilizing an evaluation criterion of weak soliton peaks.

Index Terms—dual-comb mode locking, Lyot filter, time-stretch DFT, evolutionary algorithm, neural network

I. INTRODUCTION

DUAL-COMB technologies involve utilizing two coherent optical pulse trains with a small frequency difference in their repetition rates, which can offer capabilities for fast measurements, high resolution, and high sensitivity in the fields of precise ranging [1-2] and molecular spectroscopy [3-4]. Normally, the realization of dual combs generally requires two separate and mutually coherent mode-locked lasers, which makes the source expensive, complicated, and bulky. To broaden the applicability of dual-comb technology, in 2008, K. Kieu proposed the first all-fiber bidirectional single-cavity, Erbium-doped ring-shaped laser, offering a more compact and cost-efficient solution for

generating dual combs [5]. Compared to combining two independent optical combs, employing a single-cavity dual-comb laser eliminates the need for additional stabilization approaches to lock the phases of the two pulse trains. Moreover, since these two mode-locked pulse trains share a common laser cavity, a high mutual coherence is achieved due to common-mode noise cancellation [6].

The primary methods for generating single-cavity dual combs fundamentally rely on the concept of "multiplexing", wherein the cavity is constructed to permit the simultaneous oscillation of pulses with distinct characteristics along a single propagation dimension [7], such as wavelength-multiplexing [8-9], polarization-multiplexing [10-11], direction-multiplexing [12-13], and pulse shape-multiplexing [14]. And the wavelength-multiplexing is a straightforward approach to augmenting the optical channel capacity in fiber lasers. However, the generation of single-cavity dual combs with these methods always relies on manual adjustments including precise control of intracavity polarization and gain-to-loss ratio [15]. The intricate interplay of intracavity dispersion, nonlinear dynamics, and environmental perturbations collectively induces instability in the dual-comb formation. Thus, establishing and maintaining the dual-comb mode locking within a single cavity remains a challenge, which restricts the practical utility of dual combs.

In response to these challenges, intelligent mode-locked techniques based on artificial intelligence and electric polarization controllers have been developed. Recently, genetic algorithms, deep reinforcement learning, and neural networks have been extensively applied to the intelligent control of ultrafast fiber lasers, and they have enhanced their reliability and efficiency in various applications [16-18]. In the process of intelligent mode locking, real-time acquisition of the current laser output spectrum is beneficial for accurately assessing the state of the laser system. Reinforcement learning emphasizes interaction with the environment, and by receiving rewards from the reward function, the optimal policy can be learned [19-20]. In 2024, soft actor-critic (SAC) reinforcement learning was utilized by A. Kokhanovskiy et al. for generating a harmonic mode-locked regime. The training procedure lasted 45 hours and the SAC algorithm typically took six steps to adjust the voltage in about a minute [21]. This approach requires a long time in training, thus may not be suitable for certain applications [22]. Additionally, the complexity of the nonlinear dynamics in dual-comb mode locking causes difficulties in establishing evaluation criteria. Consequently,

This work was supported by the National Natural Science Foundation of China (Grant Nos. 62475175), Opening Foundation of Key Laboratory of Laser & Infrared System (Shandong University), Ministry of Education.

Pan Guo, Yuan Gao, Yongjie Pu, and Sha Wang are with the College of Electronics and Information Engineering, Sichuan University, 610064, Chengdu, China.

Zhigang Zhao, Zhenhua Cong are with the School of Information Science and Engineering, and Shandong Provincial Key Laboratory of Laser Technology and Application, Shandong University, 266237, Qingdao, China.

† Corresponding author: Sha Wang (email: shawang@scu.edu.cn)

most of the current research on intelligent mode locking focuses on single-wavelength systems, with relatively fewer studies on dual-wavelength systems. To the best of our knowledge, there are only two such studies currently. In 2023, G. Pu et al. demonstrated the first intelligent single-cavity dual-comb fiber laser by combining the real-time intelligent control and the memory-aided intelligent searching (MAIS) algorithm. Employing a field-programmable gate array (FPGA), and two digital-to-analog converters enabled MAIS can locate a desired solution in a mean time of only 2.48 seconds [23]. However, with the existence of harmonic mode locking and temporal asynchrony, the mode-locked state of dual combs cannot be directly judged accurately relying solely on fitness function to calculate the inter-pulse margin during multiple sampling processes. This increases the total search time. Q. Yan et al. also reported an automatic mode locking in a dual-wavelength soliton fiber laser. An oscilloscope and an optical spectrum analyzer (OSA) were used simultaneously to record temporal pulse trains and spectral information. By using a two-stage genetic algorithm, the laser kept a stable dual-wavelength mode locking for hours [24]. The time taken to implement dual-wavelength mode locking has not been mentioned.

In this work, we report an intelligent single-cavity dual-comb mode-locked fiber laser based on time-stretch dispersive Fourier transform (DFT). To avoid the utilization of the bulky OSA with slow speed, an oscilloscope is used to receive DFT spectra in real time, which combines time-domain and spectral information. To elevate the performance of the laser output, a two-part evaluation criterion containing a fitness function and a CNN-Transformer network is utilized. It ensures that both global and local characteristics of the time-stretch spectrum are comprehensively considered, which leads to a more

accurate assessment of various mode-locked states. The utilized datasets exclusively consist of synthetically generated time-stretch DFT spectra, that can leave out the early collection of empirical data and improve the universality of the model. Based on the evaluation criterion, a developed EA is proposed to achieve intelligent mode locking of the dual-comb state. This EA is designed to electronically drive the paddle-based motorized polarization controllers (MPCs) and enable the optimal six-parameter search with a fitness function. The employed fitness function is capable of locating dual-comb mode locking. High-order harmonic mode locking can be accurately distinguished according to their spectral information. During the process of searching different mode-locked states automatically, a mode-locking library supporting real-time updates is built, which includes different mode-locked states, fitness functions, and angles of each paddle in the current state. The establishment of the mode-locked library allows the direct location of various mode-locking states without repeating the optimization algorithm. Multiple experiments have shown that the mode-locked library can be established within 3 minutes. Subsequently, the saved angles in the library can be directly used to achieve the corresponding dual comb mode-locked states, with an average time of less than 2 seconds, which is the fastest record according to our best knowledge.

II. EXPERIMENTAL SETUP OF THE INTELLIGENT DUAL-COMB FIBER LASER

The configuration of the intelligent dual-comb fiber laser is shown in Figure 1. The fiber laser is based on an all-fiber ring-cavity mode-locked with a nonlinear polarization rotation (NPR). A 2.5-m polarization-maintaining erbium-doped fiber

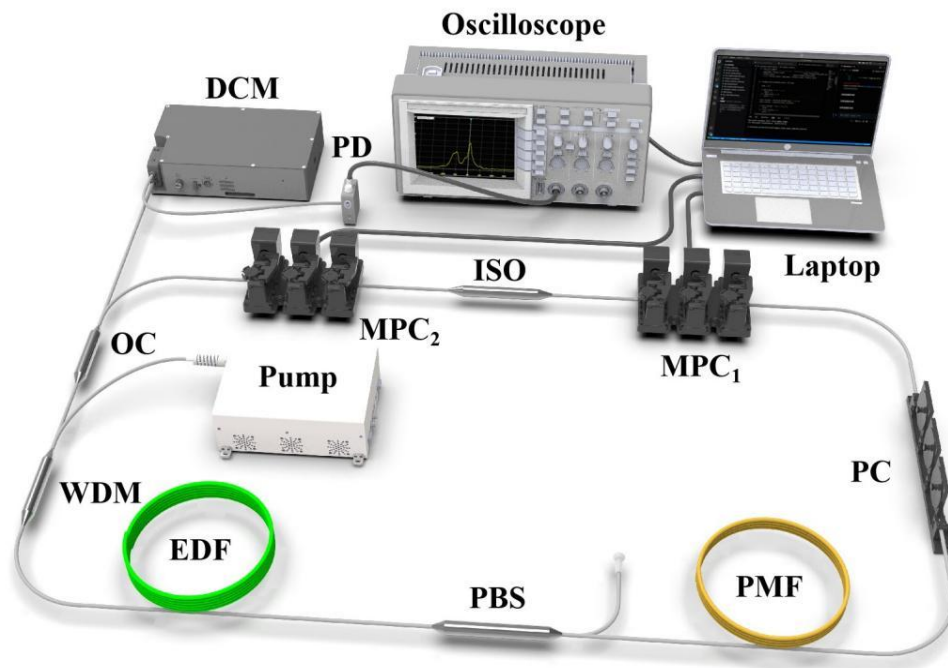


Fig. 1. The experimental setup of the intelligent single-cavity dual-comb mode-locked. laser.

(PM-EDF) with a calculated second-order dispersion of 28 ps²/km constitutes the gain medium, pumped by a 980-nm laser diode through a 980/1550 wavelength division multiplexer (WDM). A polarization-dependent isolator (PD-ISO) ensures the unidirectional transmission of light in the fiber, which together with two MPCs facilitates the NPR mode locking. The minimum step size of these two MPCs is 0.12°, and the paddle rotation angle is between 0° and 160°. The maximum rotation speed can reach 400°/sec with open loop operation. Moreover, in order to obtain dual-comb mode locking with asynchronous pulse trains, a specific intra-cavity optical filtering effect should be established. In this laser cavity, a separate PBS-PMF-PC structure is adopted. The polarization-dependent loss of the PBS and PC combined with the birefringence from 30-cm polarization-maintaining fibers can produce the Lyot filtering effect. As the central wavelength difference of two pulse trains in a dual-comb mode locking, a slight difference in their group velocities exists owing to the group velocity dispersion (GVD) of the optical fiber. And the formation of dual-comb pulse trains is significantly influenced by the dual-wavelength net gain spectrum, which depends on the balance of gain, loss, and the filtering effect. The total length of the laser cavity is ~17 m, corresponding to the fundamental repetition rate of ~12 MHz. The net cavity dispersion is ~-0.308 ps² at 1550 nm which means the mode-locked laser operates in the anomalous regime. Approximately 90% of the laser energy stays within the ring cavity by using an output coupler (OC), while the rest is utilized for characterizing laser mode-locked states and feedback control.

The output laser is propagated through a time-stretch DFT setup containing a dispersion compensation module (DCM) which provides a total accumulated dispersion of DL = -654 ps/nm. After that, the laser pulse will get stretched considerably, in order that the spectral information is mapped into the time-domain trains. A balance photodetector is used to detect the time-stretch DFT output signal, temporal pulse trains containing spectral information can be captured directly on the oscilloscope, with a resolution of $\Delta\lambda = 1 / (DL \times BW) = 0.3$ nm, where BW is the bandwidth of the balance photodetector. A laptop that runs EA and is connected to the oscilloscope can receive pulse signals in real time. And then it sends new control commands generated by the EA to electrically control six paddles of the two MPCs directly to achieve polarization control.

III. PROCESS OF THE INTELLIGENT SEARCHING

A. Two-part evaluation criterion

Establishing an excellent evaluation criterion is the key premise of intelligent search. The evaluation criterion of the individual's competitiveness has two parts: fitness function and neural network classification. Firstly, regarding the fitness function, it is observed that dual-comb mode locking may be achieved directly in the rare chance. Therefore, a dual-comb fitness function is also evaluated together with the single-wavelength fitness. When the laser output is closer to the

target state, the fitness corresponds to a higher value. We are looking for the parameters that generate solutions with the maximum total pulse energy, the number of stable pulses in the same time window, and noise intensity. The dual-region count scheme is adopted to judge the pulse trains preliminary [25]. Moreover, two intensity thresholds T_1 and T_2 are set, where $T_1 > T_2$. T_1 is built for the desired pulse count. T_2 is a limitation that noise should not surpassed. Specifically, the DFT spectrum on the oscilloscope greater than T_1 is considered as effective pulses, and those less than T_2 are considered as noises. The fitness function can be constructed as follows:

$$Fitness = I_{pulse} - \alpha |C_{real} - C_{ideal}| - \beta I_{noise} \quad (1)$$

Where the first term of the fitness is the sum intensity of the pulse I_{pulse} within a fixed time window; The second term represents the deviation punishment for the pulse count with a scale factor α , where C_{real} and C_{ideal} denote the real pulse count and the ideal pulse count of target mode-locked state, respectively; The third term stands for the punishment of noise I_{noise} and its weight β , which can show the stability of the current mode-locked state to a certain extent. The record length and acquisition time of the oscilloscope are 10K Sa and 400 ns, respectively. Five fundamental mode-locked pulse periods can be observed completely. Consequently, when the value of C_{ideal} is set to 5 and 10, Equation (1) denotes the single-wavelength mode-locked fitness and the dual-comb mode-locked fitness, respectively. We carry out multiple experiments for different weight combinations, to balance the influence of all components in the fitness function. α and β are set to 0.2 and 0.01, respectively.

However, in the dual-comb mode-locked state, the two temporal pulse trains periodically overlap because of the temporal asynchrony. As a result, certain dual-comb signals on the oscilloscope will appear to be very similar to those of single-wavelength mode-locked states. Such minor discrepancies will reduce the evaluating accuracy of the fitness function. Moreover, harmonic mode locking is also observed during the intelligent adjustment. In particular, the pulse trains of the second-order harmonic and dual-comb mode locking are very similar, this makes it difficult to efficiently distinguish with the fitness function.

Therefore, the second evaluation of the individual's competitiveness, a CNN-Transformer network, is proposed to classify the one-dimensional time-stretch DFT spectra in time domain. The training datasets of the CNN-Transformer network are completely provided by numerical simulations of the Ginzburg-Landau equation [26]:

$$\frac{\partial u}{\partial z} + i\beta_2 \frac{\partial^2 u}{\partial T^2} = i\gamma |u|^2 u + \frac{g}{2} u + \frac{g}{2\Omega_g^2} \frac{\partial^2 u}{\partial T^2} \quad (2)$$

where u is the complex envelop of the pulse trains, the attenuation coefficient of fiber $\alpha = 0.3$. The second-order dispersion in the fiber of Yb-doped fiber β_{2_YDF} and single mode fiber β_{2_SMF} are 26.2 fs²/mm and 24.7 fs²/mm, respectively. The nonlinear parameters of Yb-doped fiber γ_{YDF} and single mode fiber γ_{SMF} are 4.7e-3w⁻¹km⁻¹ and 5.1e-3w⁻¹km⁻¹.

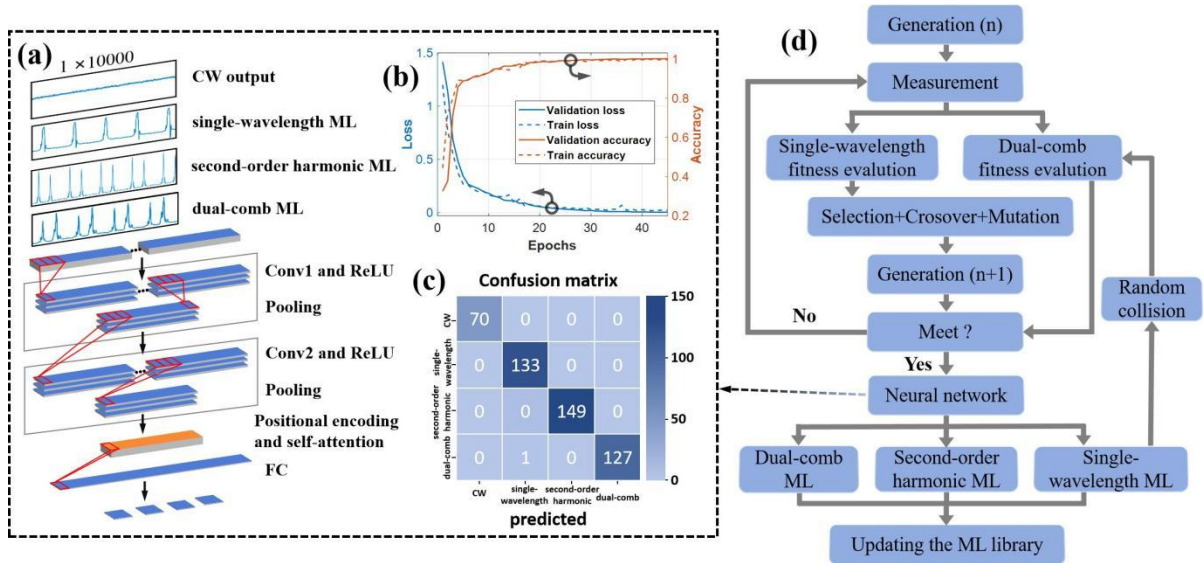


Fig. 2. (a) The classification network structure of the CNN-Transformer network. (b) The curves of the loss and accuracy over epochs in the training process. (c) Confusion matrix for the CNN-Transformer network of 4 classifications. (d) The principle of the developed EA for achieving different states of mode locking containing single-wavelength mode locking, second-order harmonic mode locking, and dual-comb mode locking.

¹, respectively. The nonlinear parameters of the Yb-doped fiber γ_{YDF} and single mode fiber γ_{SMF} are $1.7e^{-3}w^{-1}km^{-1}$ and $1.7e^{-3}w^{-1}km^{-1}$, respectively. Ω_g is the gain bandwidth, and g is the gain coefficient. The proposed dual-comb fiber laser system utilizes the wavelength-multiplexed mechanism, so simple spectrum splicing can effectively reconstruct the spectral information of the dual-comb mode locking. According to Equation (2), the propagation of pulses with central wavelengths at 1536 nm and 1561 nm in weakly birefringent optical fibers can be described. The initial noise field can evolve to a stable pulse during about 200th cycles. The simulated spectra are loaded onto a computer-generated time-domain ideal pulse with an interval of about 80 ns and a window size of 400 ns. By randomly scaling the width and intensity of the spectra, changing the initial pulse position, and adding background noise and spectral perturbation, 800 simulated time-stretch DFT spectra of single wavelength mode locking, dual-comb mode locking, and second-order harmonic mode locking are generated respectively. The continuous wave (CW) output can be generated by background noise with different intensities. The time-stretch DFT spectra generated by computer simulation can replace the signal collected in the experiment very well, as presented in Supplementary Section S1.

The network structure is shown in Figure 2(a). The model begins with a CNN module, consisting of two 1D convolutional layers with ReLU activation and max-pooling operations. Then the positional encoding of the Transformer is added to this representation to retain sequential information. Finally, the output is classified through a fully connected layer. Convolutional layers in CNN are excellent at extracting local features (e.g., spikes or small variations) in pulse trains, while the positional encoding and self-attention in Transformer can extract the global features. Additionally, The CNN reduces the pulse train length by downsampling, which helps the

Transformer operate on a smaller input and leads to faster training and inference. Using the generated time-stretch DFT spectra as datasets, a high classification accuracy can be achieved. The DFT spectra are divided into the training, validation, and test sets in a 7:1.5:1.5 ratio. The accuracy and loss results of the train and validation are demonstrated in Figure 2(b). The accuracy of the validation sets of the model reaches 99.79% within 50 epochs, while the accuracy of the training sets is 100%. From the confusion matrix depicted in Figure 2(c), it can be observed that the periodic overlap resulting from temporal asynchrony occasionally presents a challenge to its correct classification. In addition, we classify the experimental DFT spectra with this trained network and found that the accuracy is close to 100%. Overall, excellent classification outcomes are achieved due to the robust and property data processing capabilities of the CNN-Transformer network. Because of the different spectral characteristics of harmonic mode-locked pulses and dual-comb mode-locked pulses, it can be clearly mapped to the oscilloscope after time stretch, see Supplementary Section S2 for details. Thus, the second-order harmonic, as well as the single-wavelength and the dual-comb mode-locked state can be accurately distinguished. Even though higher-order harmonic mode locking above the third order is not observed due to the limitation of pump power, it is still possible to quickly search for high-order harmonic mode locking based on the spectral information contained in the time-stretch DFT pulses, as well as by properly setting the ideal pulse count of the target mode-locked state C_{ideal} in the fitness function of Equation (1). During the entire optimization process, laser outputs corresponding to different mode-locked states are not collected in advance. Therefore, this approach not only does not require experimental prior data but also enhances the universality of the model across various fiber laser systems.

B. Principle of the developed EA

According to the proposed evaluation criterion, the intelligent searching of different mode-locked states is achieved via a developed EA, and the detailed algorithmic frame is shown in Figure 2(d). In our case, the optimization algorithm, neural network classification, and the mode-locked library building or updating are tightly fused, so that the searching speed and accuracy are enhanced. EA is a class of optimization techniques inspired by the principles of biological evolution, and it is characterized by their ability to handle a wide range of optimization problems, including those with large search spaces and complex fitness landscapes [27]. In this proposed algorithm, a group of individuals is assigned randomly by the developed EA in the initial generation. And each individual has six genes, associated with the six control voltages of two MPCs. Then the user-defined fitness functions of each existing individual are calculated by collecting the dispersed consecutive waveform of time-stretch pulses through the oscilloscope. In general, single-wavelength fitness is used for achieving automatic single-wavelength mode locking. Subsequently, the EA generates the next generation by breeding individuals from the preceding generation, with selection based on fitness evaluation and the “roulette wheel” selection mechanism to determine the chosen individuals corresponding to laser output states, thereby preserving their superior genetic traits. New individuals are created by the crossover of two randomly selected parents, essentially exchanging their genes. In order to prevent falling into the local optimal mode-locked state, and ignoring the potential better state, a mutation probability is appointed to change the genes of children’s generation. The iteration continues until the required optimal mode-locked state is found. After that, a random collision algorithm that aims to realize the dual-comb mode locking is implemented on the basis of achieving single-wavelength mode locking. Random rotation angles with Gaussian probability distribution between -3° and 3° are selected in the process of random collision. This angle selection method can improve the search speed while ensuring search accuracy. We also set a threshold of 20 times random collisions. When the dual-comb mode locking is not found after the threshold number is exceeded, the EA will continue to iterate to find the next single-wavelength mode locking.

In order to further enhance the efficiency and accuracy of the optimization procedure, the EA is developed by subdividing rotation angles for MPCs, which allows for a smaller initial population to find desired mode-locked states. Since MPCs use stress-induced birefringence to dynamically control the output polarization state when the required angle that is between the current angle α_c and the target angle α_t will be missed and the search time will be increased by using the traditional search process. To overcome this, the improved EA algorithm will further divide α_c and α_t in a step of 1° , calculating the fitness function in real time during the continuous search process. When the fitness value surpasses the existing stored value, the new fitness will be saved immediately and the subsequent searching of the current genes will also be interrupted.

C. Building mode-locked library

To prevent repetitive searching of mode locking in the same laser, we build a library containing the fitness function for different stable mode-locked states and the six angles of MPCs. Depending on the initial angles of MPCs’ paddles, after multiple experiments, it is verified that the library can be built up within 3 minutes. The data in the library supports real-time updating of new mode-locked states and reading of all states. Nevertheless, the birefringence of fiber lasers is highly sensitive to environmental disturbances such as bend, twist, anisotropic stress, temperature, and so on, which have a considerable influence on mode-locked dynamics. Therefore, the library needs to be rebuilt when the birefringence in the laser cavity changes. The frequency of library rebuilding depends on the stability of the operating environment. After the mode-locked library loses effectiveness, it only takes a few minutes to rebuild the library. Reading the saved angles can directly achieve the corresponding mode-locked state, with an average time of less than 2 seconds.

IV. LASER PERFORMANCE

It is found that during the intelligent adjustment, most of the time is consumed by the mechanical motion of MPCs. In contrast, the time consumed in each step of the developed EA can be negligible. By using a laptop with an Intel i7 CPU and an NVIDIA GTX 1070 GPU, the well-trained CNN-Transformer network only needs 0.02 seconds to classify each collected time-stretch DFT spectrum in the intelligent control process.

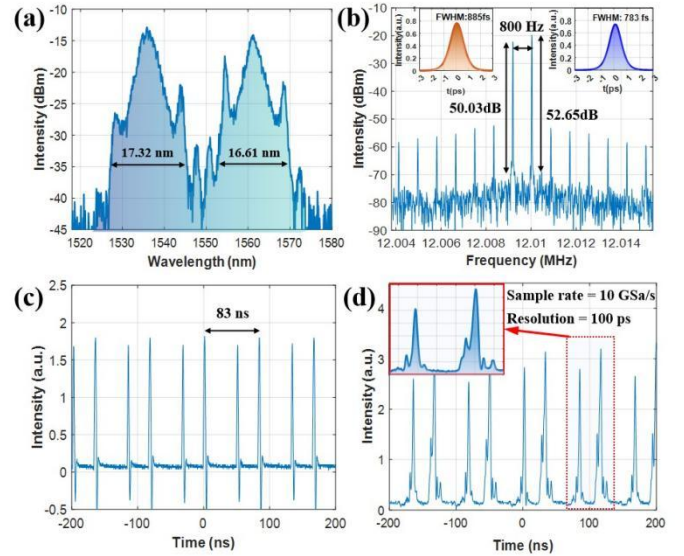


Fig. 3. Output characteristics of the intelligent dual-comb fiber laser. (a) Optical spectrum of the dual-comb mode-locked state. (b) RF spectrum with beat frequency, the left and right insets present the autocorrelation trace of solitons centered at 1536 nm and 1561 nm, respectively. (c) Time-domain pulse trains of the dual-comb mode-locked state. (d) Time-stretch DFT spectrum, inset: local view of a peak in a single period.

Figure 3 depicts the output characteristics of the intelligent dual-comb fiber laser. As shown in Figure 3(a), the spectral widths of separated mode-locked pulses with central

wavelengths of 1535.83 nm and 1561.26 nm are 17.32 nm and 16.61 nm, respectively. As the GVD characteristics of the fiber are different, additionally, self-phase modulation (SPM), which is influenced by the intracavity nonlinear coefficient and pulse intensity, will alter the pulse phase, thereby leading to a broader spectrum at 1536-nm mode locking. The intensity and position of Kelly sidebands depend on the balance of the dispersion, nonlinearity, and intracavity loss. Therefore, at 1561-nm mode locking, due to the presence of anomalous dispersion and the cumulative instability of periodic modulation caused by residual dispersion, Kelly sidebands are more likely to emerge. Due to the significant differences in optical spectra, we have found that using the different single-wavelength time-stretch DFT spectra collected in the experiment can also achieve the classification of different single-wavelength mode-locked states, see Supplementary Section S3 for details. The total output power is about 2 mW under a pump power of 220 mW. The RF spectrum can be seen in Figure 3(b), two repetition-rate signals can be found around 12.0 MHz, and the corresponding repetition-rate difference is about 800 Hz. In addition, the signal-to-noise ratios of both repetition rates are all over 50 dB, and the linewidth of the beat RF signal is about 2.34 Hz with the 1 Hz resolution bandwidth. They signify the stability of the asynchronously mode-locked pulses and the relatively good coherence between the two solitons. The orange inset on the left and the blue inset on the right present the second-harmonic generation autocorrelation trace of output solitons centered at 1536 nm and 1561 nm, respectively. By using a custom WDM, their pulse duration measured by autocorrelator is about 885 fs and 783 fs, respectively. The time-bandwidth products for the 1536 nm and 1561 nm pulses are 1.9491 and 1.6012, respectively, indicating that the pulses are chirped. The employment of the Lyot filter allows for the realization of single soliton mode locking at a higher pump power [9], so the phenomenon of multiple solitons caused by pulse splitting is not observed. The temporal oscilloscope waveform of the dual-comb pulses is shown in Figure 3(c), with a measured pulse period of ~ 83 ns. Figure 3(d) displays the one-dimensional spectra after time-stretch DFT, the inset presents the local view within a single time period. The sample rate and resolution of the oscilloscope are set to 10 GSa/s and 100 ps, respectively. It can be seen that time stretching causes the pulse width to expand from the femtosecond level to the nanosecond level, which allows the pulse to be properly unfolded in the time domain and accurate spectral information is obtained based on dispersion.

V. STABILITY MAINTENANCE

Besides ensuring that intelligent algorithms can efficiently search for and classify various mode-locked states, maintaining the stability of these states over prolonged operation is equally crucial. The spectrum changes of the mode-locked states at the central wavelengths of 1536 nm and 1561 nm can be seen in Supplementary Section S4 for details. They are easy to maintain the operation for over 6 hours. However, compared with single-wavelength mode locking, dual-comb mode-locked states, whose performance is highly dependent on the delicate balance between intracavity

dispersion and birefringence, is more difficult to maintain stable operation. To counteract interference from external environmental factors and prevent optimized dual-comb mode-locked states from experiencing a decline in quality or loss of mode locking, we propose a stability maintenance algorithm for dual-comb mode locking based on random collision.

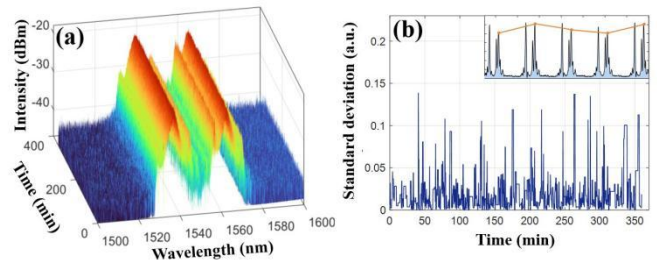


Fig. 4. (a) The stability maintenance results of dual-comb mode locking. (b) Changes of the standard deviation of pulse peak values in the process of stability maintenance, inset: details of the soliton peak selection.

The spectrum changes during the stable operation of the dual-comb mode-locked state for over 6 hours are shown in Figure 4(a) by utilizing the stability maintenance algorithm. The evaluation and specific processes of this algorithm are detailed as follows. In the dual-comb mode-locked states, two solitons with different center spectra will travel with different group velocities. Therefore, when one of the solitons is triggered, another one will periodically move on the oscilloscope. It is observed in the experiment that the triggered soliton is usually the dominant one while the moving soliton is usually weaker. This is related to the balance between the intracavity gain and loss in the laser and the setting of the Lyot filter. In this work, solitons with central wavelengths of 1561 nm and 1536 nm are the dominant soliton and weak soliton, respectively. The stable operation of weak solitons is the key to maintaining the dual-comb state. Using the dominant solitons within about 5 periods as position reference, the standard deviations of several weak solitons peaks are calculated as an evaluation criterion in real time. As shown in Figure 4(b), changes of the standard deviation in the weak soliton peaks are recorded within 6 hours, and the inset depicts a detailed example of weak soliton peak selection. In this process, the case of soliton overlap is ignored to increase the accuracy of judgment. Once the standard deviation is observed to exceed the threshold of 0.08, the stability maintenance algorithm with random collision is activated. The rotation angle of random collision rotates is a Gaussian probability distribution between -1° and 1° . After each random adjustment, the standard deviation of the output signal is recalculated to assess the effect of the collision. If the standard deviation remains above the threshold, the system counteracts the previous rotation by reversing the paddle to its original position. This reset ensures that the state of the system does not drift irreversibly, maintaining the consistency of the parameter space. Subsequently, a new random collision adjustment is initiated, and the process iterates. This iterative scheme continues until the standard deviation drops below the threshold, indicating that the system has returned to a stable

dual-comb state. This approach ensures a robust restoration of the dual-comb state while maintaining precision, as the iterative process balances randomness with reversibility.

VI. CONCLUSION

In this work, we demonstrate an intelligent single-cavity dual-comb mode-locked fiber laser. A two-part evaluation criterion containing a fitness function and a CNN-Transformer network is proposed to elevate dual-comb mode-locked states. The input datasets corresponding to various mode-locked states are obtained by simulation, which circumvents the need for over-reliance on specific experimental datasets. Then a developed EA is utilized to optimize the fitness function and control paddle-based MPCs to find the desired mode-locked state. After that, a library supporting real-time updating and reading is built to store the fitness functions for different stable mode-locked states and the six angles of MPCs. The mode-locked library can be set up within a 3-minute duration. Reading the saved angles can directly achieve the corresponding mode-locked state, with an average time of less than 2 seconds. In addition, a new evaluation criterion combined with a random collision algorithm is used to achieve the stable maintenance of the dual-comb mode locking. For subsequent work, we plan to further study the intelligent control and stability of the frequency of the dual-comb laser, and apply it to practical applications such as absorption spectrum measurement and fiber sensing.

REFERENCES

- [1] E. D. Caldwell, L. C. Sinclair, N. R. Newbury, and J. Deschenes, "The time-programmable frequency comb and its use in quantum-limited ranging," *Nature*, vol. 610, no. 7933, pp. 667-673, Oct. 2022, doi: 10.1038/s41586-022-05225-8.
- [2] J. Fellinger, *et al.*, "Simple approach for extending the ambiguity-free range of dual-comb ranging," *Optics Letters*, vol. 46, no. 15, pp. 3677-3680, Aug. 2021, doi: 10.1364/OL.427816.
- [3] B. Cho, T. H. Yoon, and M. Cho, "Dual-comb spectroscopy of molecular electronic transitions in condensed phases," *Physical Review A*, vol. 97, no. 3, pp. 033831, Mar. 2018, doi: 10.1103/PhysRevA.97.033831.
- [4] G. Millot *et al.*, "Frequency-agile dual-comb spectroscopy," *Nature Photonics*, vol. 10, no. 1, pp. 27-30, Dec. 2016, doi: 10.1038/nphoton.2015.250.
- [5] K. Kieu, and M. Mansuripur, "All-fiber bidirectional passively mode-locked ring laser," *Optics Letters*, vol. 33, no. 1, pp. 64-66, Jan. 2008, doi: 10.1364/OL.33.000064.
- [6] Z. Wang, *et al.*, "Cavity-enhanced photoacoustic dual-comb spectroscopy," *Light: Science & Applications*, vol. 13, no. 1, pp. 11, Jan. 2024, doi: 10.1038/s41377-023-01353-6.
- [7] X. Zhao, Z. Zheng, Y. Liu, G. Hu, and J. Liu, "Dual-wavelength, bidirectional single-wall carbon nanotube mode-locked fiber laser," *IEEE Photonics Technology Letters*, vol. 26, no. 17, pp. 1722-1725, Jun. 2014, doi: 10.1109/LPT.2014.2332000.
- [8] Y. Pu, M. Fan, Q. Shen, P. Guo, Y. Gao, and S. Wang, "Mode-locking and wavelength-tuning of a NPR fiber laser based on optical speckle," *Optics Letters*, vol. 49, no. 13, pp. 3686-3689, Jul. 2024, doi: 10.1364/OL.528656.
- [9] Y. Pu, *et al.*, "Yb-doped mode-locked fiber laser with a hybrid structure of NPR and a Lyot filter as the saturable absorber," *Optics Letters*, vol. 49, no. 8, pp. 2149-2152, Apr. 2024, doi: 10.1364/OL.516495.
- [10] Z. Ding, G. Wang, and F. Xu, "Highly birefringent D-shaped micro-fiber device for high-repetition-rate-difference single-cavity dual-comb generation," *Journal of Lightwave Technology*, vol. 42, no. 10, pp. 3877-3883, Feb. 2024, doi: 10.1109/JLT.2024.3368514.
- [11] M. Kowalczyk, L. Sterczewski, X. Zhang, V. Petrov, Z. Wang, and J. Sotor, "Dual-comb femtosecond solid-state laser with inherent polarization-multiplexing," *Laser & Photonics Reviews*, vol. 15, no. 8, pp. 2000441, Jun. 2021, doi: 10.1002/lpor.202000441.
- [12] Y. Liu, *et al.*, "Self-starting and repetition-rate-difference tunable dual combs in a bidirectional mode-locked fiber laser," *Optics & Laser Technology*, vol. 177, pp. 111178, Oct. 2024, doi: 10.1016/j.optlastec.2024.111178.
- [13] N. Prakash, S. W. Huang, and B. Li, "Relative timing jitter in a counterpropagating all-normal dispersion dual-comb fiber laser," *Optica*, vol. 9, no. 7, pp. 717-723, Jul. 2022, doi: 10.1364/OPTICA.458339.
- [14] Y. Liu, X. Zhao, G. Hu, C. Li, B. Zhao, and Z. Zheng, "Unidirectional, dual-comb lasing under multiple pulse formation mechanisms in a passively mode-locked fiber ring laser," *Optics Express*, vol. 24, no. 19, pp. 21392-21398, Sep. 2016, doi: 10.1364/OE.24.021392.
- [15] U. Andral, R. S. Fodil, F. Amrani, and F. Billard, "Fiber laser mode locked through an evolutionary algorithm," *Optica*, vol. 2, no. 4, pp. 275-278, Mar. 2015, doi: 10.1364/OPTICA.2.000275.
- [16] P. Guo, M. Fan, H. Li, K. Liu, Y. Pu, and S. Wang, "Intelligent laser emitting and mode locking of solid-state lasers using human-like algorithms," *Laser & Photonics Reviews*, vol. 18, no. 8, pp. 2301209, Apr. 2024, doi: 10.1002/lpor.202301209.
- [17] J. Girardot, F. Billard, A. Coillet, É. Hertz, and P. Grelu, "Autosetting mode-locked laser using an evolutionary algorithm and time-stretch spectral characterization," *IEEE Journal of Selected Topics in Quantum Electronics*, vol. 26, no. 5, pp. 1-8, Apr. 2020, doi: 10.1109/JSTQE.2020.2985297.
- [18] J. Li, *et al.*, "The soft actor-critic algorithm for automatic mode-locked fiber lasers," *Optical Fiber Technology*, vol. 81, pp. 103579, Dec. 2023, doi: 10.1016/j.yofte.2023.103579.
- [19] Q. Yan, *et al.*, "Low-latency deep-reinforcement learning algorithm for ultrafast fiber lasers," *Photonics Research*, vol. 9, no. 8, pp. 1493-1501, Jun. 2021, doi: 10.1364/PRJ.428117.
- [20] C. Sun, E. Kaiser, S. L. Brunton and J. N. Kutz, "Deep reinforcement learning for optical systems: A case study of mode-locked lasers," *Machine Learning: Science and Technology*, vol. 1, no. 4, pp. 045013, Oct. 2020, doi: 10.1088/2632-2153/abb6d6.
- [21] A. Kokhanovskiy, *et al.*, "Multistability manipulation by reinforcement learning algorithm inside mode-locked fiber laser," *Nanophotonics*, vol. 13, no. 16, pp. 2891-2901, Apr. 2024, doi: 10.1515/nanoph-2023-0792.
- [22] F. Edoardo, H. A. Loughlin, and C. Stoughton, "Controlling optical-cavity locking using reinforcement learning," *Machine Learning: Science and Technology*, vol. 5, no. 3, pp. 035027, Jul. 2024, doi: 10.1088/2632-2153/ad638f.
- [23] G. Pu, R. Liu, C. Luo, Y. Song, H. Mu, and W. Hu, "Intelligent single-cavity dual-comb source with fast locking," *Journal of Lightwave Technology*, vol. 41, no. 2, pp. 593-598, Nov. 2022, doi: 10.1109/JLT.2022.3220258.
- [24] Q. Yan, *et al.*, "Machine learning based automatic mode-locking of a dual-wavelength soliton fiber laser," *Photonics*, vol. 11, no. 1, pp. 47, Dec. 2024, doi: 10.3390/photonics11010047.
- [25] G. Pu, L. Yi, L. Zhang, and W. Hu, "Intelligent programmable mode-locked fiber laser with a human-like algorithm," *Optica*, vol. 6, no. 3, pp. 362-369, Mar. 2019, doi: 10.1364/OPTICA.6.000362.
- [26] Y. Lyu, J. Li, Y. Hu, Y. Wang, C. Wei, Y. Liu, "Theoretical comparison of NPR and hybrid mode-locked soliton thulium-doped fiber lasers," *IEEE Photonics Journal*, vol. 9, no. 1, pp. 1-11, Jan. 2017, doi: 10.1109/JPHOT.2017.2653860.
- [27] T. Bäck, and H. P. Schwefel, "An overview of evolutionary algorithms for parameter optimization," *Evolutionary computation*, vol. 1, no. 1, pp. 1-23, Mar. 1993, doi: 10.1162/evco.1993.1.1.1.

Supplemental File

S1. The time-stretch DFT spectra of dual comb generated by the computer

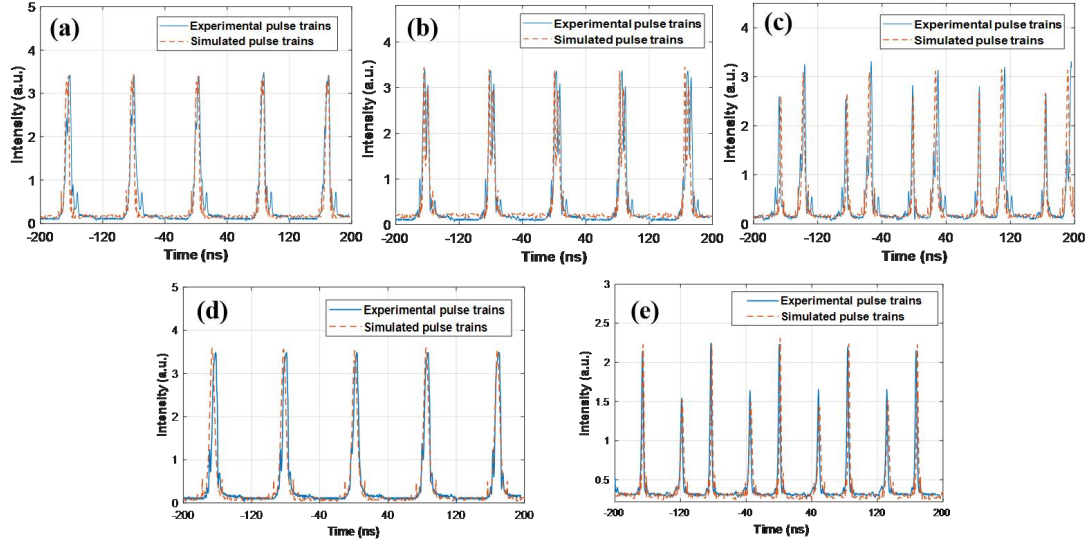


Fig. S1. Comparison of time-stretch DFT signals generated by computer simulation and experimental measurement. (a) Complete overlap, (b) partial overlap, (c) complete separation, (d) single-wavelength mode locking and (e) harmonic mode locking.

The time-stretch DFT spectra generated by the computer are compared with those collected in the experiment. Figure S1 (a), (b), and (c) select the cases where the time-stretch DFT spectra completely overlap, partially overlap, and completely separate, respectively. Figure S1 (d) and (e) select the time-stretch DFT spectra of single-wavelength mode locking and harmonic mode locking, respectively. It can be seen that the time-stretch DFT spectra generated by computer simulation can replace the signal collected by the experiment very well.

S2. Time-stretch DFT spectrum of the harmonic mode-locked state

The measured second-order harmonic time-stretch DFT spectrum is shown in Figure S2(a), and it can be seen that they are very similar to the DFT spectra of dual-comb mode locking. Thus during the process of using the evolutionary algorithm with a fitness function of Equation (1), it is difficult to distinguish between dual-comb mode locking and second-order harmonic mode locking using only pulse count. Although harmonic mode locking has periodic pulse repetition in the time domain, unlike dual-comb mode locking, multiple pulses within the same period all have the same spectral information. After passing through the DCM, adjacent second-order harmonic mode locking time-stretch DFT pulses have similar profiles, as shown in Figure S2(b). In dual-comb mode locking, due to the different spectral information of two solitons within the same period, significant differences can be exhibited after time stretching, as shown in Figure S2(c).

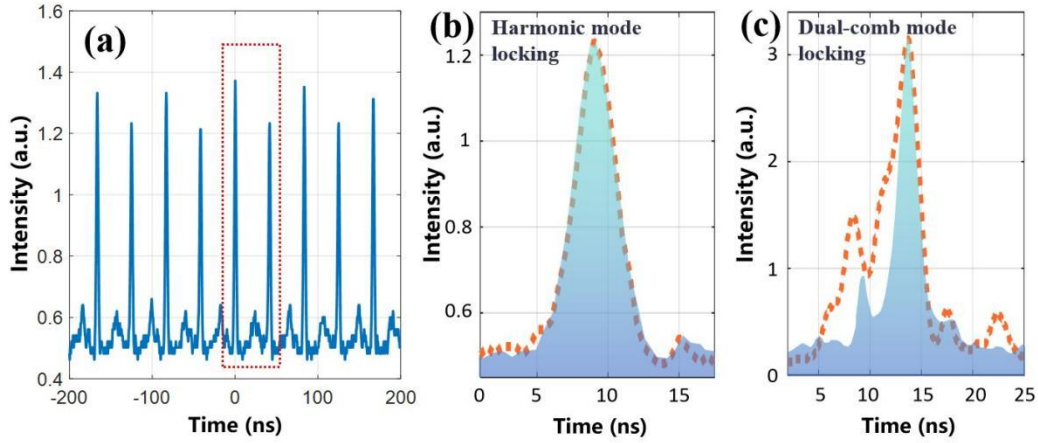


Fig. S2. (a) Time-stretch DFT spectrum of the harmonic mode-locked state. After normalization and shift processing, the overlapping curves of adjacent pulses of (b) harmonic mode locking and (c) dual-comb mode locking.

S3. Classification of 1536-nm and 1561-nm single-wavelength mode-locked states

After the time stretch of the dispersion compensation module, these spectral characteristics will map to the DFT time-domain pulse trains. Benefiting from these characteristics, we also achieve the automatic tuning of single-wavelength mode locking with different central wavelengths. In the experiment, 800 DFT pulse trains with central wavelengths at 1536 nm and 1561 nm are collected, respectively. Combined with the previously simulated CW output, second-order harmonic and the dual-comb DFT pulse trains together as the input datasets, a 5-class neural network is trained without any changes to the network structure or hyperparameters. Figure S3(a) depicts that the accuracy of the validation sets of the model reaches 99.67% within 100 epochs, while the accuracy of the training sets is 100%. As shown in Figure S3(b), in addition to the periodic overlap of dual-comb pulse trains, the time-stretch signals of the single-wavelength mode locking centered at 1536 nm and 1561 nm are similar, which results in occasional errors in classification.

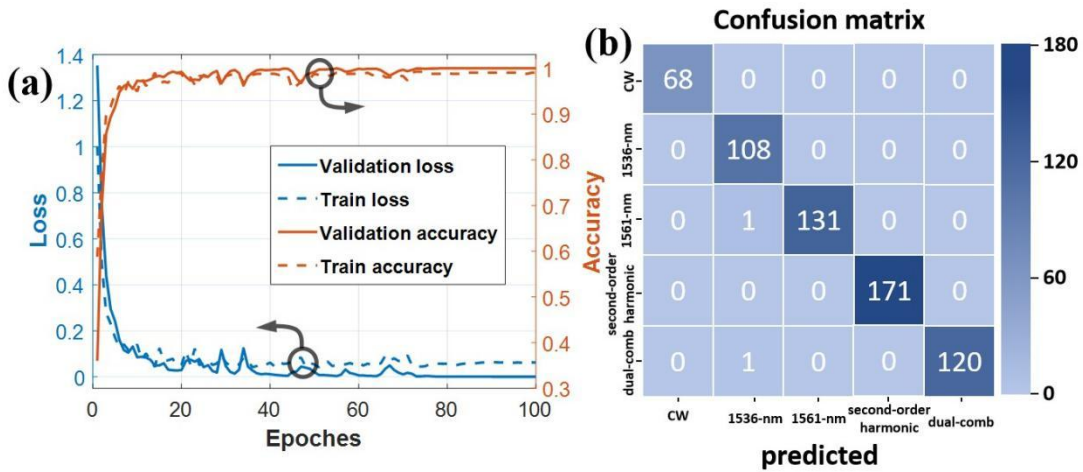


Fig. S3. (a) The curves of the loss and accuracy over epochs in the training process. (b) Confusion matrix for the CNN-Transformer hybrid model of 5 classification.

S4. The spectrum changes of single-wavelength mode-locked states

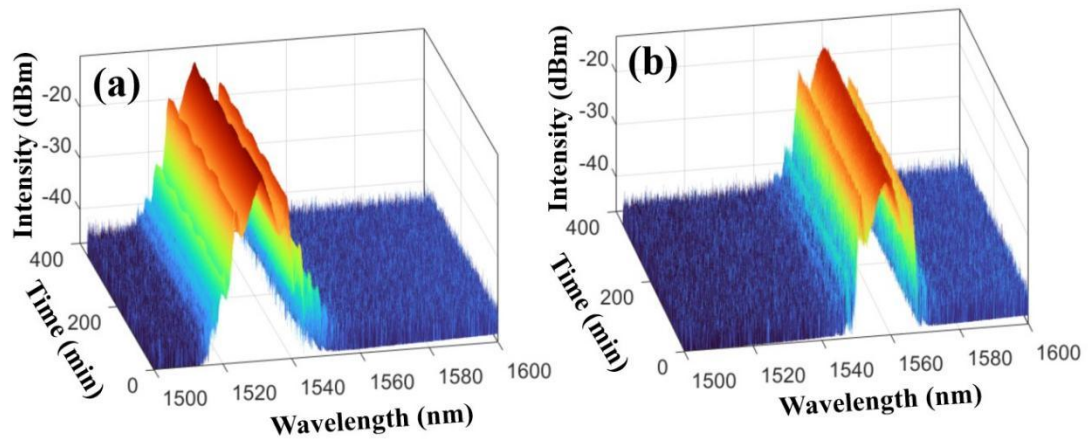


Fig. S4. The stability maintenance results of different mode-locked states including single-wavelength mode locking centered at (a) 1536 nm and (b) 1561 nm.

The stable single-wavelength mode-locked states are obtained by using the proposed developed evolutionary algorithm with the fitness function of single-wavelength mode locking. The CNN-Transformer network can be used to classify different single-wavelength mode-locked states such as 1536-nm mode locking and 1561-nm mode locking. The spectral changes of the proposed laser at the central wavelength of 1536 nm and 1561 nm are shown in Figure S4. They are easy to maintain for more than 6 hours of operation.